AIAA Journal
Vol. 48, No. 11, November 2010

Technical Notes

Proposed Boundary Conditions for Gust–Airfoil Interaction Noise

Jae Wook Kim,* Alex S. H. Lau,† and Neil D. Sandham‡
University of Southampton, Southampton, England SO17 1BJ, United Kingdom

DOI: 10.2514/1.J050428

I. Introduction

THE sponge zone technique is part of the recent progress in artificial boundary conditions for the computation of compressible flow and sound [1]. It is generally represented by a term $-\sigma(q - q_{\text{ref}})$ that is added to the right-hand side of governing equations, where σ is a free parameter to control the strength of the sponge, q is a flow variable and q_{ref} is the reference solution desired in the sponge. Although this technique is widespread, primarily to remove outflow disturbances and wave reflections from the boundaries, it is also useful for embedding inflow perturbations. There are some examples of inflow perturbations via sponges shown by Freund [2], Zhao et al. [3], Bodony and Lele [4], and Bodony [5] for transmitting instability waves into jets and mixing layers. Meanwhile, Bodony [5] used this technique to represent an acoustic source at the center of an ambient field. However, existing publications are limited to unbounded domains without a solid body inside. The present work demonstrates its implementation in the presence of a solid body (an airfoil in particular) for direct computation of gust–airfoil interaction noise.

Gust–airfoil interaction is one of the contributing aerodynamic noise sources of wind turbines [6] and aircraft turbofan engines [7]. Currently, there exists some fundamental work done in this area using computational approaches [8–12]. From a numerical perspective, in order to tackle more realistic problems (especially in high-frequency gusts), there should be an efficient and reliable strategy to embed the inflow disturbances without causing reflections from the boundaries. This paper proposes a modified form of the sponge technique for these purposes with an additional interest in achieving low computational cost (smaller domain size and fewer grid cells) compared with conventional airfoil calculations. The outcome of the present work will form a basis for low-cost calculations of gust–airfoil interaction, especially aimed at low-noise airfoil/blade design in realistic gust profiles.

II. Boundary Conditions for Gust–Airfoil Interaction

The present work is based on a Joukowski airfoil subject to a two-dimensional periodic vortical gust, as shown in Fig. 1 (see [10,11]). The gust velocity field is given by

$$u_{\text{gust}} = u_\infty(1+\delta) \quad \text{and} \quad v_{\text{gust}} = -u_\infty \delta \tag{1}$$

with

$$\delta = \delta(x,y,t) = -k_1 \cos[k_2(x+y-u_\infty t)/L]$$

where L represents the airfoil chord, and the constants are set to $k_1 = \sqrt{2}/100$ and $k_2 = 2.0$. The freestream Mach number is $M_\infty = 0.5$. The Joukowski airfoil used has a 12% thickness and a 2% camber, and the angle of attack (AOA) is 2°. Figure 1 also shows the computational setup with the overall domain size represented by L_Ω and the sponge thickness by L_S.

The fully nonlinear compressible Euler equations with the sponge forcing terms are used in the present work, which is expressed in two-dimensional generalized coordinates as

$$\frac{\partial \mathbf{Q}^*}{\partial t} + \frac{\partial \mathbf{E}^*}{\partial \xi} + \frac{\partial \mathbf{F}^*}{\partial \eta} = -\frac{a_\infty}{L}\mathbf{S}^* \tag{2}$$

where a_∞ is the ambient speed of sound (hence, L/a_∞ is a characteristic time scale). The asterisks represent properties in the generalized coordinates. The spatial derivatives in Eq. (2) are calculated by fourth-order pentadiagonal compact finite difference schemes [13]. The solution is advanced in time by using a classical fourth-order Runge–Kutta scheme. Numerical stability is maintained by sixth-order compact filters [14].

A. Conventional Sponge Conditions

In the conventional implementation of sponge conditions, the forcing term in Eq. (2) is set to

$$\mathbf{S}_{\text{old}} = \sigma(\mathbf{Q} - \mathbf{Q}_{\text{ref}}) = \sigma \begin{pmatrix} \rho - \rho_\infty \\ \rho u - \rho_\infty u_{\text{gust}} \\ \rho v - \rho_\infty v_{\text{gust}} \\ \rho e_t - \rho_\infty e_{t\text{gust}} \end{pmatrix} \tag{3}$$

with

$$e_{t\text{gust}} = \frac{p_\infty}{(\gamma-1)\rho_\infty} + \frac{u_{\text{gust}}^2 + v_{\text{gust}}^2}{2}$$

where $\sigma = \sigma(x,y)$ maintains zero in the physical zone and grows smoothly in the sponge zones to a specified maximum at the boundaries. Equation (3) forces density and pressure to their ambient values, and it forces velocity to the gust function given by Eq. (1) in all four sponge zones. The basic sponge profile with smooth blending over the corners is given by

$$\sigma(x,y) = \sigma_0\{1+\cos[\pi A(x)B(y)]\}/2 \tag{4}$$

for

$$x \in [x_{\min}, x_{\max}] \qquad \text{and} \qquad y \in [y_{\min}, y_{\max}]$$

with

$$\begin{cases} A(x) = 1 - \max[1-(x-x_{\min})/L_s, 0] - \max[1-(x_{\max}-x)/L_s, 0], \\ B(y) = 1 - \max[1-(y-y_{\min})/L_s, 0] - \max[1-(y_{\max}-y)/L_s, 0]. \end{cases}$$

A suitable sponge coefficient σ_0 for this particular problem is found in Sec. III.B. A typical sponge profile based on Eq. (4) is plotted in Fig. 2. The conventional implementation may yield significant errors in far-field sound intensity, as shown in Sec. III.C.

Presented as Paper 2010-0839 at the 48th AIAA Aerospace Sciences Meeting, Orlando, FL, 4–7 January 2010; received 8 February 2010; revision received 30 July 2010; accepted for publication 2 August 2010.

*Lecturer, School of Engineering Sciences; j.w.kim@soton.ac.uk. Senior Member AIAA.

†Postgraduate Research Student, School of Engineering Sciences. Member AIAA.

‡Professor, School of Engineering Sciences. Senior Member AIAA.

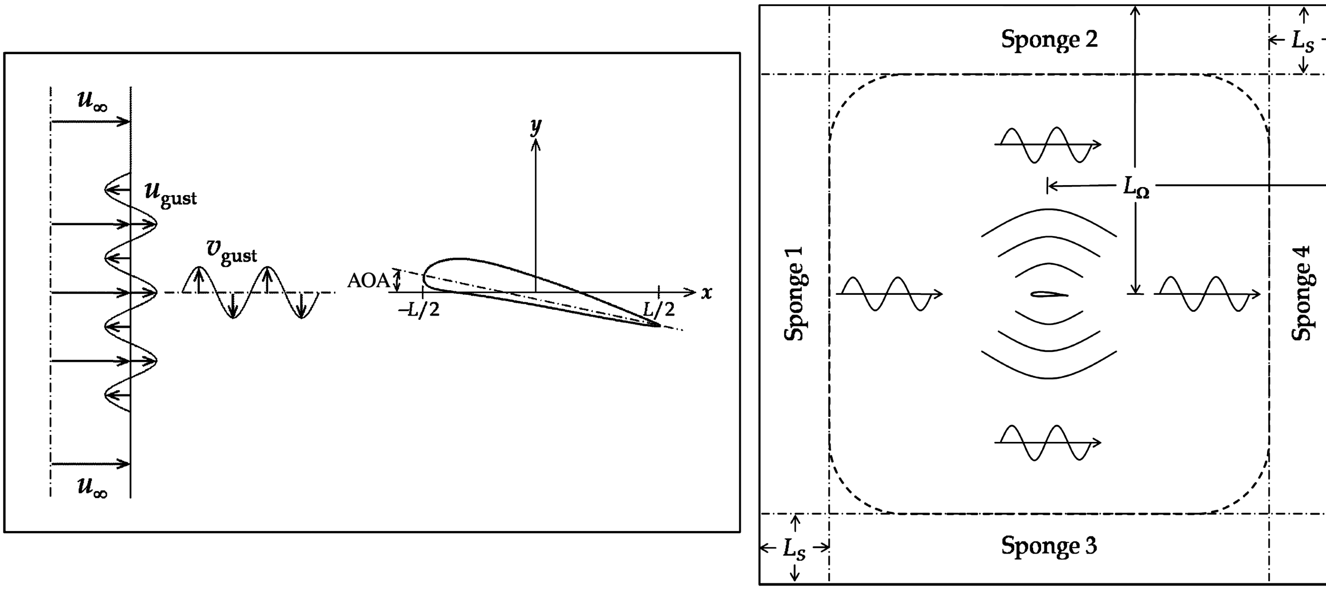

Fig. 1 The schematic of gust–airfoil interaction (left) and computational setup (right).

B. Proposed Sponge Conditions

This paper proposes two additional features as a modification to the existing sponge technique: 1) forcing pressure instead of total energy (multiplied by density), in the last row of Eq. (3); and 2) introducing a weighting factor λ into the velocity forcing terms. The modification is represented by

$$\mathbf{S}_{\text{new}} = \sigma \begin{pmatrix} \rho - \rho_\infty \\ \lambda(\rho u - \rho_\infty u_{\text{gust}}) \\ \lambda(\rho v - \rho_\infty v_{\text{gust}}) \\ p - p_\infty \end{pmatrix} \tag{5}$$

where the sponge profile $\sigma = \sigma(x, y)$ is the same as Eq. (4). The modified forcing term no longer conforms with the conventional form: $\mathbf{S}_{\mathbf{new}} \neq \sigma(\mathbf{Q} - \mathbf{Q}_{\mathbf{ref}})$; however, each component is still dimensionally consistent. Modification 1 is intended to focus more on the pressure forcing, since forcing applied to the total energy overrides the density and velocity forcing that already take place in the first three rows of Eq. (3). Modification 2 gives better control over the velocity forcing, depending on the problem type.

The weighting factor λ in Eq. (5) is given as a function of x (in the direction of mean flow) for this problem, which yields stronger velocity forcing in the upstream area than downstream:

$$\lambda = \lambda(x) = (1 - \varepsilon)[1 - \tanh(x/L)]/2 + \varepsilon \tag{6}$$

where the center of the body is located at $x = 0$. The weighting factor decreases from 1 to ε as x increases, where ε ($\ll 1$) is an ad hoc constant to refine the minimum level of forcing. In this paper, ε is set to zero. This weighting factor effectively modifies the profile of velocity forcing, while the density and pressure forcing maintain the original profile. The modified profile of velocity forcing (σ multiplied by λ) is plotted in Fig. 2, by which the strength is concentrated in sponge 1 and diminished through sponges 2 and 3 to zero in sponge 4. The controlled velocity forcing helps avoid excessive constraint on the outflow condition where the velocity distribution no longer follows the prescribed gust function. It might be necessary to increase ε in Eq. (6) with an extended exit sponge in Navier–Stokes calculations where the body generates wakes causing significant acoustic reflections at the exit boundary.

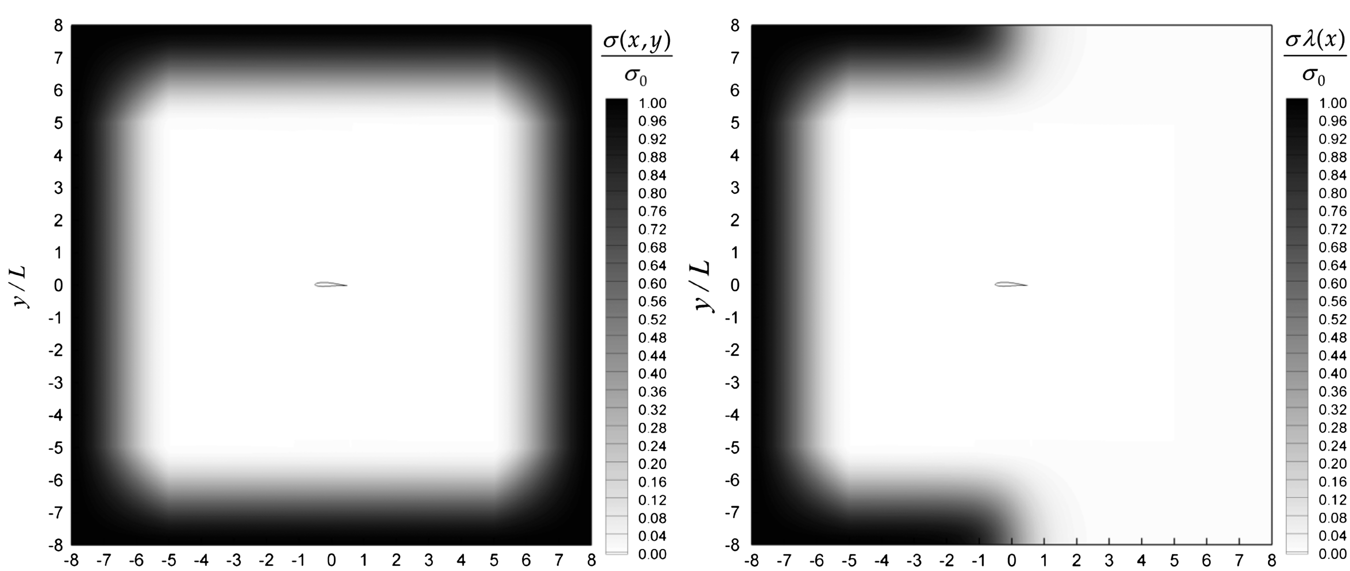

Fig. 2 Conventional (left) and proposed (right) sponge profiles for velocity forcing by Eqs. (4) and (6) ($L_\Omega = 8L$ and $L_S = 3L$).

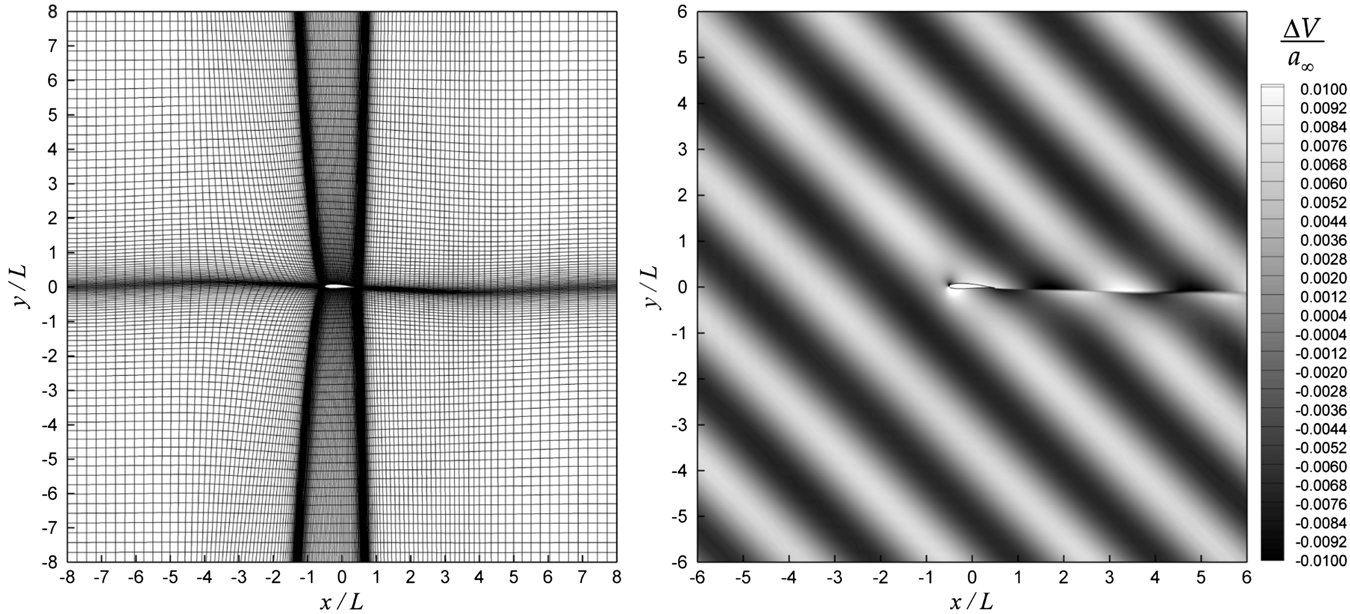

Fig. 3 Baseline grid (left) and contour plots of perturbed velocity (right).

III. Numerical Tests and Results

This section provides the result of the current calculations. The baseline grid used is shown in Fig. 3, which contains 17,472 cells in total, where 64 are on each side of the airfoil, 52 are upstream and downstream, and 52 are upward and downward. The smallest cell located at the leading edge has $\Delta x/L = 0.0075$ and $\Delta y/L = 0.0053$. The time step size is determined by the Courant–Friedrichs–Lewy number of 0.95. Each calculation runs until $a_\infty t/L = 50$, after which the mean flow has travelled 25 times the chord, where M_∞ is ramped from 0 to 0.5 until $a_\infty t/L = 10$ by using a moving frame technique that avoids spurious solutions from the initial condition.

The final data are collected within the last period of the gust for postprocessing the solutions. It has been checked that the statistics of the solutions are fully converged and do not change thereafter. The perturbed velocity field due to the gust is plotted in Fig. 3, where $V = (u^2 + v^2)^{1/2}$, $\Delta V = V - \langle V \rangle$, and $\langle\ \rangle$ denotes averaging in time.

Parametric tests of domain size L_Ω, sponge thickness L_S, sponge coefficient σ_0, and the number of grid cells have been performed to check their influence on the solutions. The results are compared with two benchmark solutions by [10,11]. Wang et al. [10] used a second-order method with 643,744 cells and $L_\Omega = 20L$. Golubev and Mankbadi [11] used a fourth-order method with 54,125 cells (for the current gust frequency) and $L_\Omega = 7L$. The current work employs 17,472 cells to obtain the same level of accuracy in both the near field and the far field with the help of the proposed sponge conditions.

A. Mean Pressure on Airfoil Surface

Time-averaged pressure $\langle p \rangle$ distributions on the airfoil surface are examined across various values of the sponge parameters. Figure 4 shows the variation of $\langle p \rangle$ with L_Ω. It can be seen that the $\langle p \rangle$ profiles converge to the reference solution as L_Ω increases, and the deviation is within 0.5% for $L_\Omega \geq 8L$. It is observed that the profiles undergo little change with different values of $L_S \geq 1L$. Also, the profile is hardly affected by $\sigma_0 \geq 2$. It is found that $L_\Omega \geq 8L$, $L_S \geq 1L$, and $\sigma_0 \geq 2$ are suitable to accurately reproduce the mean wall pressure.

B. Aeroacoustic Properties

The sponge parameters are reexamined for aeroacoustic properties. To maximize the computational efficiency, $L_\Omega = 8L$ (the smallest domain size available from the earlier test) is maintained. It has been checked that profiles of the root-mean-squared (rms) pressure fluctuation $\langle \Delta p^2 \rangle^{1/2} (\Delta p = p - \langle p \rangle)$ on the airfoil surface are in almost perfect agreement with the reference solution [10] for all the values of L_S and σ_0 recommended earlier. The intensity of

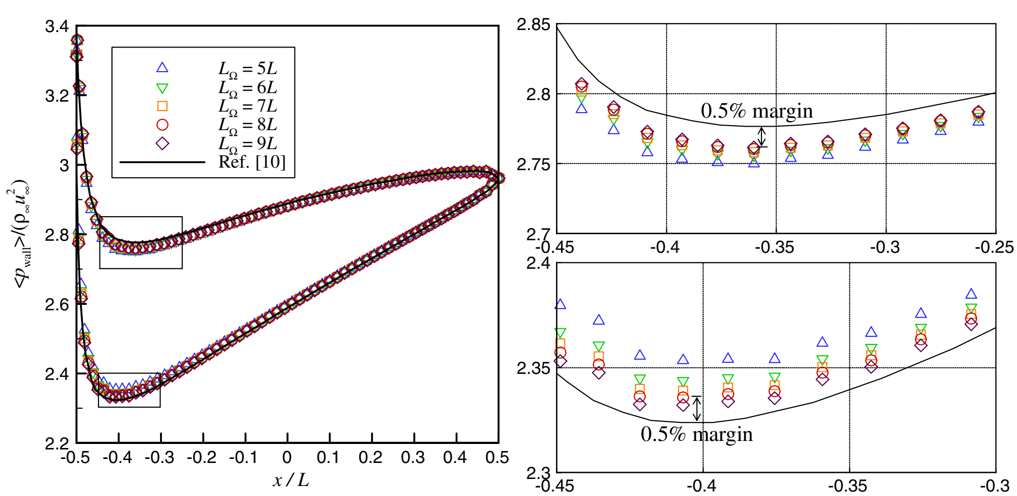

Fig. 4 Mean wall pressure with different values of L_Ω ($L_S = 2L$ and $\sigma_0 = 4$).

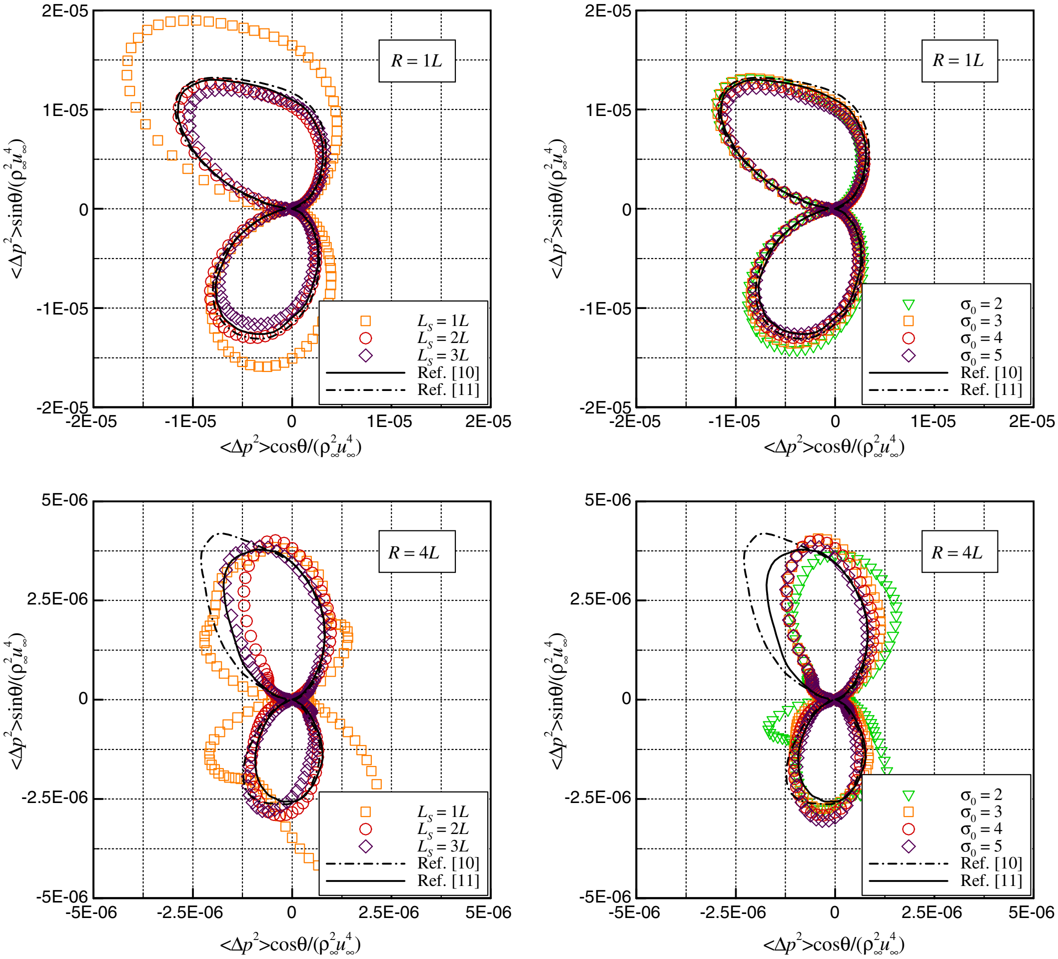

Fig. 5 Sound intensity on $R = 1L$ (top) and $R = 4L$ (bottom), with different values of L_S (left, $\sigma_0 = 4$) and σ_0 (right, $L_S = 2L$) ($L_\Omega = 8L$).

propagated sound $\langle \Delta p^2 \rangle$ measured on a circle of $R = 1L$ and $R = 4L$ is shown in Fig. 5. The circles are defined by $R = (x^2 + y^2)^{1/2}$ from the center of the airfoil $(x, y) = (0, 0)$. Figure 5 shows that the current solutions agree very well with the reference solutions for $L_S \geq 2L$ and $\sigma_0 \geq 3$, given $L_\Omega = 8L$. However, the cases with $L_S = 1L$ or $\sigma_0 = 2$ seem to be less effective, particularly in the far field ($R = 4L$). To this end, an optimal combination of $(L_\Omega, L_S, \sigma_0) = (8L, 2L, 4)$ is suggested for both the near-field aerodynamics and the far-field acoustics. This combination has also been applied to a finer grid that has four times as many cells (69,888 in total) with half the Δx and Δy as the baseline grid (twice the resolution uniformly in every direction). The refined grid yields almost perfect agreement with the baseline grid case.

C. Comparison with Conventional Sponge Conditions

The same parametric tests previously mentioned have been made with the conventional sponge conditions for comparison purposes. The conventional ones provide almost identical results with the proposed ones in terms of the mean pressure and the rms pressure fluctuation on the airfoil surface. However, a significant difference is found in the far-field acoustic solutions, as shown in Fig. 6 in contrast

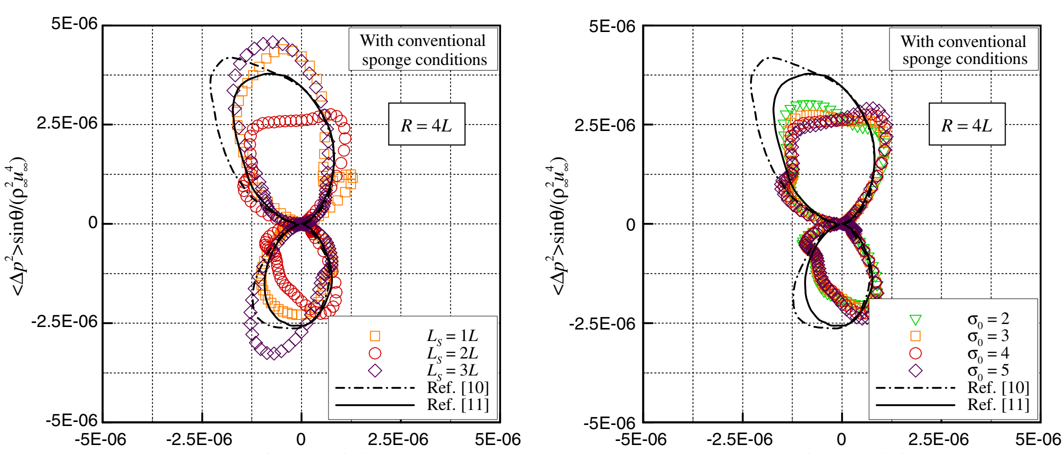

Fig. 6 Applying conventional sponge conditions: sound intensity on $R = 4L$ with different values of L_S (left, $\sigma_0 = 4$) and σ_0 (right, $L_S = 2L$) ($L_\Omega = 8L$).

with Fig. 5. The conventional ones yield inconsistent results: for example, an underprediction on $R = 1L$ but an overprediction on $R = 4L$. They also show inconsistent behavior with L_S, where the solution suddenly collapses at $L_S = 2L$, generating a significantly rugged profile that is not improved by applying different values of σ_0, as shown in Fig. 6. This is presumably due to their excessive forcing (blockage effect), since all the variables are forced in the entire sponge area. The blockage effect may be diminished by using a larger domain, but this requires more computational effort.

IV. Conclusions

Modified sponge boundary conditions have been successfully implemented for the calculation of gust–airfoil interaction noise. The new sponge treatment is proven to perform more accurately and consistently than the conventional sponge conditions, particularly for long-range propagation of sound waves. The proposed boundary conditions enable the use of a significantly smaller domain size and fewer grid cells compared with previous benchmark cases at $k_2 = 2.0$. An optimal combination of the sponge parameters $(L_\Omega, L_S, \sigma_0) = (8L, 2L, 4)$ that provides the most efficient calculation for this particular problem is achieved through rigorous parametric tests. The enhanced efficiency of the present treatment makes the calculation of gust–airfoil interaction noise more feasible, particularly considering three-dimensional applications with realistic multiple gust components superimposed.

Acknowledgments

The authors gratefully acknowledge the support of the Industrial Collaborative Awards in Science and Engineering Studentship by the Engineering and Physical Sciences Research Council and Vestas Technology Research and Development, United Kingdom, in partnership with South East England Development Agency.

References

[1] Colonius, T., "Modelling Artificial Boundary Conditions for Compressible Flow," *Annual Review of Fluid Mechanics*, Vol. 36, 2004, pp. 315–345.
doi:10.1146/annurev.fluid.36.050802.121930

[2] Freund, J. B., "Noise Sources in a Low-Reynolds-Number Turbulent Jet at Mach 0.9," *Journal of Fluid Mechanics*, Vol. 438, 2001, pp. 277–305.
doi:10.1017/S0022112001004414

[3] Zhao, W., Frankel, S. H., and Mongeau, L., "Large Eddy Simulations of Sound Radiation from Subsonic Turbulent Jets," *AIAA Journal*, Vol. 39, No. 8, 2001, pp. 1469–1477.
doi:10.2514/2.1497

[4] Bodony, D. J., and Lele, S. K., "On Using Large-Eddy Simulation of the Prediction of Noise from Cold and Heated Turbulent Jets," *Physics of Fluids*, Vol. 17, No. 8, 2005, p. 085103.
doi:10.1063/1.2001689

[5] Bodony, D. J., "Analysis of Sponge Zones for Computational Fluid Mechanics," *Journal of Computational Physics*, Vol. 212, No. 2, 2006, pp. 681–702.
doi:10.1016/j.jcp.2005.07.014

[6] Lutz, T., Herrig, A., Würz, W., Kamruzzaman, M., and Krämer, E., "Design and Wind-Tunnel Verification of Low-Noise Airfoils for Wind Turbines," *AIAA Journal*, Vol. 45, No. 4, 2007, pp. 779–785.
doi:10.2514/1.27658

[7] Casalino, D., Diozzi, F., Sannino, R., and Paonessa, A., "Aircraft Noise Reduction Technologies: A Bibliographic Review," *Aerospace Science and Technology*, Vol. 12, No. 1, 2008, pp. 1–17.
doi:10.1016/j.ast.2007.10.004

[8] Scott, J. R., and Atassi, H. M., "A Finite-Difference Frequency-Domain Numerical Scheme for the Solution of the Gust Response Problem," *Journal of Computational Physics*, Vol. 119, No. 1, 1995, pp. 75–93.
doi:10.1006/jcph.1995.1117

[9] Lockard, D. P., and Morris, P. J., "Radiated Noise from Airfoils in Realistic Mean Flows," *AIAA Journal*, Vol. 36, No. 6, 1998, pp. 907–914.
doi:10.2514/2.494

[10] Wang, X. Y., Himansu, A., Chang, S. C., and Jorgenson, P. C. E., "Computation of a Single Airfoil Gust Response and Gust–Cascade Interaction Using the CE/SE Method," NASA CP 2004-212954, pp. 115–126, 2004.

[11] Golubev, V. V., and Mankbadi, R. R., "Space-Time Mapping Analysis of Airfoil Response to Impinging Gust," NASA CP 2004-212954, pp. 135–140, 2004.

[12] Hixon, R., Golubev, V. V., Mankbadi, R. R., Scott, J. R., Sawyer, S., and Nallasamy, M., "Application of a Nonlinear Computational Aeroacoustics Code to the Gust-Airfoil Problem," *AIAA Journal*, Vol. 44, No. 2, 2006, pp. 323–328.
doi:10.2514/1.3478

[13] Kim, J. W., "Optimised Boundary Compact Finite Difference Schemes for Computational Aeroacoustics," *Journal of Computational Physics*, Vol. 225, No. 1, 2007, pp. 995–1019.
doi:10.1016/j.jcp.2007.01.008

[14] Kim, J. W., "High-Order Compact Filters with Variable Cut-off Wavenumber and Stable Boundary Treatment," *Computers and Fluids*, Vol. 39, No. 7, 2010, pp. 1168–1182.
doi:10.1016/j.compfluid.2010.02.007

A. Lyrintzis
Associate Editor